Advanced Robotics

ISSN: (Print) (Online) Journal homepage: https://www.tandfonline.com/loi/tadr20

A survey: dynamics of humanoid robots

Tomomichi Sugihara & Mitsuharu Morisawa

To cite this article: Tomomichi Sugihara & Mitsuharu Morisawa (2020): A survey: dynamics of humanoid robots, Advanced Robotics, DOI: 10.1080/01691864.2020.1778524

To link to this article: https://doi.org/10.1080/01691864.2020.1778524

Published online: 17 Jun 2020.

ADVANCED ROBOTICS
https://doi.org/10.1080/01691864.2020.1778524

SURVEY PAPER

OPEN ACCESS Check for updates

A survey: dynamics of humanoid robots

Tomomichi Sugihara[a,b] and Mitsuharu Morisawa[c]

[a]Preferred Networks, Inc., Chiyoda-ku, Japan; [b]Graduate School of Engineering, Osaka University, Japan; [c]National Institute of Advanced Industrial Science and Technology, CNRS-AIST JRL (Joint Robotics Laboratory), UMI3218/IRL, Tsukuba, Japan

ABSTRACT

The mathematical foundation to describe the dynamics of a humanoid mechanism is reviewed. The discussion begins with the kinematics of an anthropomorphic mechanism, followed by the equation of motion of the system and the contact mechanics that accompanies with the motions. Some compact representations of both the robot dynamics and the contact mechanics are summarized. The former is referred to as the centroidal dynamics derived from the total momenta of the system, while the latter includes the contact wrench sum and the zero-moment point. They are naturally joined as a reduced-order dynamics model derived from an approximate relationship between the center of mass and the zero-moment point. Finally, some techniques to synthesize the intended motion into the joint actuation torques under limitations of contact forces are shown. This is basically a translation of a Japanese version with some modifications and reorganizations.

ARTICLE HISTORY
Received 16 March 2020
Accepted 17 May 2020

KEYWORDS
Humanoid robot; contact mechanics; centroidal dynamics; COM-ZMP model; motion resolution control

1. Introduction

The goal of the humanoid robotics is to realize machines that behave as if they were humans, or more boldly expressing, machines with *human-like intelligence*. While the authors are fully aware of a risk to refer to the intelligence in the context of engineering, which is mathematically ill-defined, they are sure it is nothing but the intelligence that orchestrates the whole-body behavior under severe physical constraints. The body is not puppeteered by the almighty intelligence but is ruled by the strict laws of physics. In this sense, the body rather guides the intelligence. Hence, it is necessary to understand the dynamics of humanoids and model it appropriately in order to bring the human-like intelligence into engineering discussions.

This paper is basically a translation of a Japanese version [1] with some modifications and reorganizations, in which the mathematical foundation to describe the dynamics of a humanoid mechanism is reviewed. The discussion begins with the kinematics of an anthropomorphic mechanism, followed by the equation of motion of the system and the contact mechanics that necessarily accompanies with the motions. Some compact representations of both the robot dynamics and the contact mechanics are summarized. The former is referred to as the centroidal dynamics derived from the total momenta of the system, while the latter includes the contact wrench sum and the zero-moment point. They are naturally joined as a reduced-order dynamics model derived from an approximate relationship between the center of mass and the zero-moment point. Finally, some techniques to synthesize the intended motion described by a set of requirements on it with priorities into the joint actuation torques under limitations of contact forces are shown.

2. Mathematical description of the humanoid dynamics

2.1. Kinematics of an anthropomorphic mechanism

It is probably a common agreement to represent an anthropomorphic mechanism with a trunk, a pair of arms, a pair of legs and a head. The trunk is usually composed of some segments. The other parts also comprise some segments and branched from any segment of the trunk. Those parts do not form closed loops with each other though they might have inner loops. Hence, it is basically modeled as a tree-like open kinematic chain. In the modern manner of kinematics one of the segments (usually of the trunk) is regarded as a *floating-base link*, which can freely translate and rotate in the inertial frame. A convenient representation is to connect the base link with the inertial frame via 6-DOF virtual joints as depicted in Figure 1. This idea was proposed by Vukobratović and Stepanenko [2] in the early days of the field, although it had not been broadly employed for more than a decade. It was refound for satellite-type manipulators in

CONTACT Tomomichi Sugihara zhidao@ieee.org Preferred Networks, Inc., 1–6–1 Otemachi, Chiyoda-ku, Tokyo 100-0004, Japan

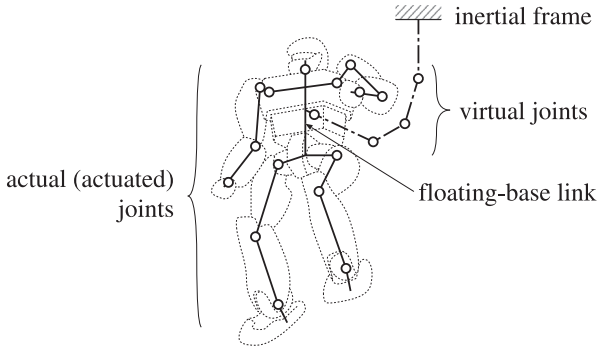

Figure 1. Kinematic structure of a humanoid with a floating-base link.

the latter half of the 1980s [3,4] and also for biped robots by Fujimoto and Kawamura [5]. Nakamura and Yamane [6] named the anthropomorphic kinematic structure *the human figure*, which can represent humanoid robots, human-formed characters in CG animations as well as real humans.

Suppose the branches do not have inner loops and all (actual) joints are actuated. The generalized coordinate to represent the robot configuration can be defined as

$$\boldsymbol{q} \stackrel{\text{def}}{=} \begin{bmatrix} \boldsymbol{q}_{\mathrm{B}}^{\mathrm{T}} & \boldsymbol{q}_{\mathrm{J}}^{\mathrm{T}} \end{bmatrix}^{\mathrm{T}}, \tag{1}$$

where

$$\boldsymbol{q}_{\mathrm{J}} \stackrel{\text{def}}{=} \begin{bmatrix} \boldsymbol{q}_0^{\mathrm{T}} & \boldsymbol{q}_1^{\mathrm{T}} & \boldsymbol{q}_2^{\mathrm{T}} & \boldsymbol{q}_3^{\mathrm{T}} & \boldsymbol{q}_4^{\mathrm{T}} & \boldsymbol{q}_5^{\mathrm{T}} \end{bmatrix}^{\mathrm{T}}, \tag{2}$$

$\boldsymbol{q}_{\mathrm{B}}$ denotes the displacement of the virtual joints of the floating-base link, and $\boldsymbol{q}_0, \ldots, \boldsymbol{q}_5$ the joint displacements of the trunk, the left arm, the right arm, the left leg, the right leg and the head, respectively. If the number of joints that independently move is n, the total degree of freedom of the mechanism with respect to the inertial frame is $n+6$.

2.2. Equation of motion of the robot

The robot motion is produced from the actuation force (joint torque), the gravitational force and the contact forces from the environment based on the following equation of motion [5,7]:

$$\begin{bmatrix} \boldsymbol{H}_{\mathrm{BB}} & \boldsymbol{H}_{\mathrm{BJ}} \\ \boldsymbol{H}_{\mathrm{BJ}}^{\mathrm{T}} & \boldsymbol{H}_{\mathrm{JJ}} \end{bmatrix} \begin{bmatrix} \ddot{\boldsymbol{q}}_{\mathrm{B}} \\ \ddot{\boldsymbol{q}}_{\mathrm{J}} \end{bmatrix} + \begin{bmatrix} \boldsymbol{b}_{\mathrm{B}} \\ \boldsymbol{b}_{\mathrm{J}} \end{bmatrix} = \begin{bmatrix} \boldsymbol{0} \\ \boldsymbol{\tau}_{\mathrm{J}} \end{bmatrix} + \begin{bmatrix} \boldsymbol{\tau}_{\mathrm{CB}} \\ \boldsymbol{\tau}_{\mathrm{CJ}} \end{bmatrix}, \tag{3}$$

where

$$\boldsymbol{H}_{\mathrm{BJ}} \stackrel{\text{def}}{=} \begin{bmatrix} \boldsymbol{H}_{\mathrm{B0}} & \boldsymbol{H}_{\mathrm{B1}} & \cdots & \boldsymbol{H}_{\mathrm{B5}} \end{bmatrix} \tag{4}$$

$$\boldsymbol{H}_{\mathrm{JJ}} \stackrel{\text{def}}{=} \begin{bmatrix} \boldsymbol{H}_{00} & \boldsymbol{H}_{01} & \cdots & \boldsymbol{H}_{05} \\ \boldsymbol{H}_{01}^{\mathrm{T}} & \boldsymbol{H}_{11} & & \boldsymbol{O} \\ \vdots & & \ddots & \\ \boldsymbol{H}_{05}^{\mathrm{T}} & \boldsymbol{O} & & \boldsymbol{H}_{55} \end{bmatrix} \tag{5}$$

$$\boldsymbol{b}_{\mathrm{J}} \stackrel{\text{def}}{=} \begin{bmatrix} \boldsymbol{b}_0^{\mathrm{T}} & \boldsymbol{b}_1^{\mathrm{T}} & \cdots & \boldsymbol{b}_5^{\mathrm{T}} \end{bmatrix}^{\mathrm{T}} \tag{6}$$

$$\boldsymbol{\tau}_{\mathrm{J}} \stackrel{\text{def}}{=} \begin{bmatrix} \boldsymbol{\tau}_0^{\mathrm{T}} & \boldsymbol{\tau}_1^{\mathrm{T}} & \cdots & \boldsymbol{\tau}_5^{\mathrm{T}} \end{bmatrix}^{\mathrm{T}}, \tag{7}$$

$\boldsymbol{H}_*$ are the inertial matrices, $\boldsymbol{b}_*$ are generalized bias forces due to the centrifugal, Coriolis and gravitational forces, and $\boldsymbol{\tau}_*$ are the joint actuation torques corresponding to $\boldsymbol{q}_*$. As common natures of mechanical systems, the inertial matrix of the whole system is positive-definite and symmetric. An additional property that is particular for the human figure is that it is doubly-bordered block-diagonal due to the branched structure, and accordingly, sparse. An efficient way to compute $\boldsymbol{H}_*$ and $\boldsymbol{b}_*$ [8] is acknowledged in the field. The number of actuation forces is n while the total DOF is $n+6$, and thus, the system is necessarily underactuated no matter how large n is. $\boldsymbol{\tau}_{\mathrm{CB}}$ and $\boldsymbol{\tau}_{\mathrm{CJ}}$ are the generalized forces due to the contact forces, which are represented as

$$\begin{bmatrix} \boldsymbol{\tau}_{\mathrm{CB}} \\ \boldsymbol{\tau}_{\mathrm{CJ}} \end{bmatrix} = \sum_{i=0}^{5} \int_{\boldsymbol{p} \in \mathcal{S}_i} \begin{bmatrix} \boldsymbol{J}_{\mathrm{CB}}^{\mathrm{T}}(\boldsymbol{p}, \boldsymbol{q}) \\ \boldsymbol{J}_{\mathrm{CJ}}^{\mathrm{T}}(\boldsymbol{p}, \boldsymbol{q}) \end{bmatrix} \boldsymbol{\sigma}(\boldsymbol{p}) \mathrm{d}s, \tag{8}$$

where $\mathcal{S}_i$ $(i = 0, \ldots, 5)$ is the contact region of the ith branch and the environment, $\boldsymbol{\sigma}(\boldsymbol{p})$ is a contact stress exerted at a point $\boldsymbol{p}$, $\mathrm{d}s$ is a infinitesimally small area at $\boldsymbol{p}$, and $\boldsymbol{J}_{\mathrm{CB}}(\boldsymbol{p}, \boldsymbol{q})$ and $\boldsymbol{J}_{\mathrm{CJ}}(\boldsymbol{p}, \boldsymbol{q})$ are Jacobian matrices that map $\dot{\boldsymbol{q}}$ to $\dot{\boldsymbol{p}}$ (of the robot-side) as

$$\boldsymbol{J}_{\mathrm{CB}}(\boldsymbol{p}, \boldsymbol{q}) \dot{\boldsymbol{q}}_{\mathrm{B}} + \boldsymbol{J}_{\mathrm{CJ}}(\boldsymbol{p}, \boldsymbol{q}) \dot{\boldsymbol{q}}_{\mathrm{J}} = \dot{\boldsymbol{p}}. \tag{9}$$

The above equation holds with respect to the countless number of all contact points $\boldsymbol{p}$ in the contact region. An efficient way to compute the Jacobian matrices [9,10] is also acknowledged. $\boldsymbol{J}_{\mathrm{CJ}}(\boldsymbol{p}, \boldsymbol{q})$ is also sparse due to the branched structure of the mechanism as well as the inertia matrix. More concretely, let us decompose the matrix as

$$\boldsymbol{J}_{\mathrm{CJ}}(\boldsymbol{p}, \boldsymbol{q}) = \begin{bmatrix} \boldsymbol{J}_{\mathrm{C0}} & \boldsymbol{J}_{\mathrm{C1}} & \cdots & \boldsymbol{J}_{\mathrm{C5}} \end{bmatrix}. \tag{10}$$

When $\boldsymbol{p} \in \mathcal{S}_i$ $(i = 0, \ldots, 5)$ and $i \neq j$ $(j = 1, \ldots, 5)$, $\boldsymbol{J}_{\mathrm{C}j} = \boldsymbol{O}$.

As $\boldsymbol{q}_{\mathrm{B}}$ denotes the 6-DOF movement of the base link, there is an equivalent mapping from $\dot{\boldsymbol{q}}_{\mathrm{B}}$ to a combination of the linear and angular velocities of the base link $\begin{bmatrix} \dot{\boldsymbol{p}}_{\mathrm{B}}^{\mathrm{T}} & \boldsymbol{\omega}_{\mathrm{B}}^{\mathrm{T}} \end{bmatrix}^{\mathrm{T}}$. In this sense, $\dot{\boldsymbol{q}}_{\mathrm{B}}$ is substitutable with the latter, and in this case, $\boldsymbol{J}_{\mathrm{CB}}(\boldsymbol{p}, \boldsymbol{q})$ is written as

$$\boldsymbol{J}_{\mathrm{CJ}}(\boldsymbol{p}, \boldsymbol{q}) = \begin{bmatrix} \boldsymbol{1} & -(\boldsymbol{p} - \boldsymbol{p}_{\mathrm{B}})\times \end{bmatrix}, \tag{11}$$

where $\boldsymbol{1}$ is an identity matrix of the corresponding size, and $\boldsymbol{v}\times$ for an arbitrary three-dimensional vector $\boldsymbol{v}$ means the outer product matrix.

2.3. Contact mechanics

The contact stress $\boldsymbol{\sigma}(\boldsymbol{p})$ in Equation (8) is produced from an interaction of the robot and the environment; when the actuation force $\boldsymbol{\tau}_{\mathrm{J}}$ is propagated in the robot body and acts to the environment at the contact point $\boldsymbol{p}$, the robot gains $\boldsymbol{\sigma}(\boldsymbol{p})$ as the reaction. It means that the behavior of the robot is not completely described only by the equation of motion of the robot but also depends on the dynamics of the environment.

While the robot body is commonly modeled as a kinematic chain, a terrain can be regarded as a huge deformable object that has almost infinite degrees of freedom. The deformation occurs in submillimeter scale in many situations, and some models for the process are available [11–14]. However, it is not necessarily a good idea to track such a tiny-scale process along with movements of the robot from the viewpoint of computation. A pragmatic way is to regard the environment as a monolithic rigid body and ignore its deformation. The following part of this section introduces techniques based on this assumption – obviously, largely deformable terrains comprising piled rocks, soils, or sands, for instance, are outside the scope of this.

Although it is assumed in Equation (8) that the contact points are distributed over contact regions, an approximation to represent them by vertices of the convex hull of the regions is often employed. This is acceptable because the set of net contact wrenches of possible contact stresses in the contact region is identical with the set of net contact wrenches of possible contact forces concentrated at the vertices under an assumption of Coulomb friction [15]. Suppose all the contact regions $\{\mathcal{S}_i\}$ $(i = 0, \ldots, 5)$ are polygonal convexes and their vertices are $\{\boldsymbol{p}_{\mathrm{C}k}\}$ $(k = 1, \ldots, N_{\mathrm{C}}$, where N_{C} is the total number of the vertices). Equation (8) is rewritten as

$$\begin{bmatrix} \boldsymbol{\tau}_{\mathrm{CB}} \\ \boldsymbol{\tau}_{\mathrm{CJ}} \end{bmatrix} = \sum_{k=1}^{N_{\mathrm{C}}} \begin{bmatrix} \boldsymbol{J}_{\mathrm{CB}k}^{\mathrm{T}} \\ \boldsymbol{J}_{\mathrm{CJ}k}^{\mathrm{T}} \end{bmatrix} \boldsymbol{f}_{\mathrm{C}k}, \tag{12}$$

where $\boldsymbol{J}_{\mathrm{CB}k}$ and $\boldsymbol{J}_{\mathrm{CJ}k}$ are matrices that map $\dot{\boldsymbol{q}}$ to $\dot{\boldsymbol{p}}_{\mathrm{C}k}$ as

$$\boldsymbol{J}_{\mathrm{CB}k}\dot{\boldsymbol{q}}_{\mathrm{B}} + \boldsymbol{J}_{\mathrm{CJ}k}\dot{\boldsymbol{q}}_{\mathrm{J}} = \dot{\boldsymbol{p}}_{\mathrm{C}k}, \tag{13}$$

and $\boldsymbol{f}_{\mathrm{C}k}$ is the contact force acting at $\boldsymbol{p}_{\mathrm{C}k}$.

Note that the contact point $\boldsymbol{p}$ is not permanent, which makes it still difficult to predict the time evolution of the overall system even with the above assumption. From Equations (3), (12) and (13), the following equation is obtained:

$$\begin{bmatrix} \boldsymbol{H}_{\mathrm{BB}} & \boldsymbol{H}_{\mathrm{BJ}} & -\boldsymbol{J}_{\mathrm{CB1}}^{\mathrm{T}} & \cdots & -\boldsymbol{J}_{\mathrm{CB}N_{\mathrm{C}}}^{\mathrm{T}} & \boldsymbol{O} & \cdots & \boldsymbol{O} \\ \boldsymbol{H}_{\mathrm{BJ}}^{\mathrm{T}} & \boldsymbol{H}_{\mathrm{JJ}} & -\boldsymbol{J}_{\mathrm{CJ1}}^{\mathrm{T}} & \cdots & -\boldsymbol{J}_{\mathrm{CJ}N_{\mathrm{C}}}^{\mathrm{T}} & \boldsymbol{O} & \cdots & \boldsymbol{O} \\ \boldsymbol{J}_{\mathrm{CB1}} & \boldsymbol{J}_{\mathrm{CJ1}} & \boldsymbol{O} & \cdots & \boldsymbol{O} & -\boldsymbol{1} & & \boldsymbol{O} \\ \vdots & \vdots & \vdots & & \vdots & & \ddots & \\ \boldsymbol{J}_{\mathrm{CB}N_{\mathrm{C}}} & \boldsymbol{J}_{\mathrm{CJ}N_{\mathrm{C}}} & \boldsymbol{O} & \cdots & \boldsymbol{O} & \boldsymbol{O} & & -\boldsymbol{1} \end{bmatrix} \begin{bmatrix} \ddot{\boldsymbol{q}}_{\mathrm{B}} \\ \ddot{\boldsymbol{q}}_{\mathrm{J}} \\ \boldsymbol{f}_{\mathrm{C1}} \\ \vdots \\ \boldsymbol{f}_{\mathrm{C}N_{\mathrm{C}}} \\ \ddot{\boldsymbol{p}}_{\mathrm{C1}} \\ \vdots \\ \ddot{\boldsymbol{p}}_{\mathrm{C}N_{\mathrm{C}}} \end{bmatrix} = \begin{bmatrix} -\boldsymbol{b}_{\mathrm{B}} \\ \boldsymbol{\tau}_{\mathrm{J}} - \boldsymbol{b}_{\mathrm{J}} \\ -\dot{\boldsymbol{J}}_{\mathrm{CB1}}\dot{\boldsymbol{q}}_{\mathrm{B}} - \dot{\boldsymbol{J}}_{\mathrm{CJ1}}\dot{\boldsymbol{q}}_{\mathrm{J}} \\ \vdots \\ -\dot{\boldsymbol{J}}_{\mathrm{CB}N_{\mathrm{C}}}\dot{\boldsymbol{q}}_{\mathrm{B}} - \dot{\boldsymbol{J}}_{\mathrm{CJ}N_{\mathrm{C}}}\dot{\boldsymbol{q}}_{\mathrm{J}} \end{bmatrix}. \tag{14}$$

The above Equation (14) has $n + 3N_{\mathrm{C}} + 6$ equations and $n + 6N_{\mathrm{C}} + 6$ unknown variables; $3N_{\mathrm{C}}$ equations are missing to be solved. If the Coulomb friction is assumed, only the following conditions are accepted for $\forall k$:

(I: stationary contact)

$$\begin{cases} \dot{\boldsymbol{p}}_{\mathrm{C}k} = \boldsymbol{0} \\ \boldsymbol{v}_k^{\mathrm{T}}\boldsymbol{f}_{\mathrm{C}k} \geq 0 \\ \|\boldsymbol{f}_{\mathrm{C}k} - (\boldsymbol{v}_k^{\mathrm{T}}\boldsymbol{f}_{\mathrm{C}k})\boldsymbol{v}_k\| \leq \mu_{\mathrm{S}k}\boldsymbol{v}_k^{\mathrm{T}}\boldsymbol{f}_{\mathrm{C}k} \end{cases} \tag{15}$$

(II: sliding)

$$\begin{cases} \dot{\boldsymbol{p}}_{\mathrm{C}k} \neq \boldsymbol{0}, \quad \boldsymbol{v}_k^{\mathrm{T}}\dot{\boldsymbol{p}}_{\mathrm{C}k} = 0 \\ \boldsymbol{f}_{\mathrm{C}k} \times \left(\boldsymbol{v}_k - \mu_{\mathrm{K}k}\frac{\dot{\boldsymbol{p}}_{\mathrm{C}k}}{\|\dot{\boldsymbol{p}}_{\mathrm{C}k}\|}\right) = \boldsymbol{0} \end{cases} \tag{16}$$

(III: separation)

$$\begin{cases} \boldsymbol{v}_k^{\mathrm{T}}\dot{\boldsymbol{p}}_{\mathrm{C}k} > 0 \\ \boldsymbol{f}_{\mathrm{C}k} = \boldsymbol{0} \end{cases}, \tag{17}$$

where $\boldsymbol{v}_k$ is the outward unit normal vector of the terrain, and $\mu_{\mathrm{S}k}$ and $\mu_{\mathrm{K}k}$ are the static and kinetic friction coefficients at $\boldsymbol{p}_{\mathrm{C}k}$, respectively. The above conditions represent the unilaterality and the friction limit of contact forces. Penetration $\boldsymbol{v}_k^{\mathrm{T}}\dot{\boldsymbol{p}}_{\mathrm{C}k} < 0$ is not acceptable. Any of Equations (15), (16) and (17) includes three independent equalities. Hence, the total number of equations balances with the number of variables when combined with Equation (14). A difficulty is that it is hard to know which condition fits the state to be evolved over time in advance. This is a typical non-smooth mechanics [16] and has been mainly studied in the context of dynamics simulations [17–25].

Equations (15), (16) and (17) define a set of acceptable combinations of $\boldsymbol{f}_{\mathrm{C}k}$ and $\dot{\boldsymbol{p}}_{\mathrm{C}k}$. On the other hand, the variable in Equation (14) includes $\boldsymbol{f}_{\mathrm{C}k}$ and $\ddot{\boldsymbol{p}}_{\mathrm{C}k}$. This gap of physical dimension causes several problems in both theoretical and practical aspects. The time evolution is not described by a differential equation but by *a differential inclusion* [26], where the time derivative of the state is included in a set-valued function. The conditions (I) and

(II) are not exclusive if $\mu_{Sk} > \mu_{Kk}$, which holds in many cases, and thus, the uniqueness of solution is not guaranteed. This is known as *Painlevé's paradox* [27,28]. The differential inclusion can be converted to a complementarity problem by assuming $\mu_{Sk} = \mu_{Kk}$ and applying an implicit discretization, and efficiently solved by off-the-shelf techniques [18]. Another issue to be addressed in practice is the numerical ill-posedness, which often leads to chatterings of the solution. Some methods to resolve this based on the regularization have been proposed [25,29–31].

As the state evolves according to the above differential inclusion, the kinematic structure of the total system collocating with the environment changes. Nakamura and Yamane [6] named it *the structure-varying kinematic chain*.

3. Centroidal dynamics

3.1. Centroidal momentum matrix

Although the equation of motion of a humanoid robot derived in the previous section is complex with many degrees-of-freedom, Miyazaki and Arimoto [32] pointed out a simple fact that the inertial movement of a biped system is decomposed into angular momenta that the center of mass produces about the supporting point and that the whole-body produces about the center of mass. Furusho and Masubuchi [33] showed a control architecture to abstract the principal mode originated from the above angular momenta. Orin et al. [34] named them *the centroidal dynamics*. Let us review a direct derivation of the centroidal dynamics from the upper part of Equation (3), which is equivalent with

$$\begin{bmatrix} \dot{\boldsymbol{h}}_{\mathrm{L}} \\ \dot{\boldsymbol{h}}_{\mathrm{A}} \end{bmatrix} + \begin{bmatrix} m\boldsymbol{g} \\ \boldsymbol{0} \end{bmatrix} = \begin{bmatrix} \boldsymbol{f}_{\mathrm{C}} \\ \boldsymbol{n}_{\mathrm{C}} - \boldsymbol{p}_{\mathrm{G}} \times \boldsymbol{f}_{\mathrm{C}} \end{bmatrix}, \tag{18}$$

where $\boldsymbol{h}_{\mathrm{L}}$ is the total linear momentum, $\boldsymbol{h}_{\mathrm{A}}$ is the total angular momentum about the center of mass (COM), m is the total mass, $\boldsymbol{p}_{\mathrm{G}}$ is the position of COM, $\boldsymbol{f}_{\mathrm{C}}$ is the net contact force, $\boldsymbol{n}_{\mathrm{C}}$ is the net contact torque about the origin, and $\boldsymbol{g}$ is the acceleration due to the gravity. This matches with a well-known fact that the rate of the total linear/angular momentum of a system is equal to the net external force/torque. The following equation is immediately derived:

$$\boldsymbol{p}_{\mathrm{G}} \times (\dot{\boldsymbol{h}}_{\mathrm{L}} + m\boldsymbol{g}) + \dot{\boldsymbol{h}}_{\mathrm{A}} = \boldsymbol{n}_{\mathrm{C}}. \tag{19}$$

$\boldsymbol{h}_{\mathrm{L}}$ and $\boldsymbol{h}_{\mathrm{A}}$ are related with $\dot{\boldsymbol{q}}$ by certain matrices $\boldsymbol{H}_{\mathrm{L}}$ and $\boldsymbol{H}_{\mathrm{A}}$, respectively, as

$$\boldsymbol{h}_{\mathrm{L}} = \boldsymbol{H}_{\mathrm{L}}\dot{\boldsymbol{q}} \tag{20}$$

$$\boldsymbol{h}_{\mathrm{A}} = \boldsymbol{H}_{\mathrm{A}}\dot{\boldsymbol{q}}. \tag{21}$$

Hence, the following identities obviously hold:

$$\begin{bmatrix} \boldsymbol{H}_{\mathrm{BB}} & \boldsymbol{H}_{\mathrm{BJ}} \end{bmatrix} \equiv \begin{bmatrix} \boldsymbol{H}_{\mathrm{L}} \\ \boldsymbol{H}_{\mathrm{A}} \end{bmatrix} \tag{22}$$

$$\boldsymbol{b}_{\mathrm{B}} \equiv \begin{bmatrix} \dot{\boldsymbol{H}}_{\mathrm{L}}\dot{\boldsymbol{q}} + m\boldsymbol{g} \\ \dot{\boldsymbol{H}}_{\mathrm{A}}\dot{\boldsymbol{q}} \end{bmatrix}. \tag{23}$$

Namely, $\boldsymbol{H}_{\mathrm{L}}$ and $\boldsymbol{H}_{\mathrm{A}}$ are nothing but a part of the inertial matrix of the system.

As Kajita et al. [35] pointed out, $\boldsymbol{H}_{\mathrm{L}}$ divided by m coincides with the COM Jacobian matrix [36]. On the other hand, $\boldsymbol{H}_{\mathrm{A}}$ was named the angular momentum Jacobian matrix in some papers [37,38], which is not appropriate since the angular momentum is not obtained by differentiating a certain quantity, while the Jacobian matrix is a derivative of a multivalued function. Orin et al. [34] called them *the centroidal momentum matrices*. Several algorithms to compute them was proposed; Tamiya et al. [39,40] applied numerical differentiation with $\mathrm{O}(n^3)$. The original Boulić et al.'s method [36] was with $\mathrm{O}(n^2)$. Sugihara's method [37] was also with $\mathrm{O}(n^2)$, though it halved the computation amount of Boulić et al.'s. Kajita et al. [35] proposed a recursive $\mathrm{O}(n)$ algorithm, which was refined by Orin et al. [34].

3.2. Reaction-null space

Yoshida and Nenchev [41] showed some important properties of $\boldsymbol{H}_{\mathrm{BB}}$ and $\boldsymbol{H}_{\mathrm{BJ}}$ as reviewed here. Let us consider a fictitious situation where the robot is floating in a gravity-free space and no external forces are applied. The robot's motion is ruled by the momentum conservation law as

$$\boldsymbol{H}_{\mathrm{BB}}\dot{\boldsymbol{q}}_{\mathrm{B}} + \boldsymbol{H}_{\mathrm{BJ}}\dot{\boldsymbol{q}}_{\mathrm{J}} = \boldsymbol{h}_{\mathrm{B0}} : \text{const.}, \tag{24}$$

where $\boldsymbol{h}_{\mathrm{B0}}$ is the initial value of linear and angular momenta. Since $\boldsymbol{H}_{\mathrm{BB}}$ is always regular,

$$\dot{\boldsymbol{q}}_{\mathrm{B}} = \boldsymbol{H}_{\mathrm{BB}}^{-1}\boldsymbol{h}_{\mathrm{B0}} - \boldsymbol{H}_{\mathrm{BB}}^{-1}\boldsymbol{H}_{\mathrm{BJ}}\dot{\boldsymbol{q}}_{\mathrm{J}}. \tag{25}$$

Namely, the reaction of $\dot{\boldsymbol{q}}_{\mathrm{J}}$ contributes to $\dot{\boldsymbol{q}}_{\mathrm{B}}$ in addition to the effect of the initial momenta. The larger the singular value of $\boldsymbol{H}_{\mathrm{BB}}^{-1}\boldsymbol{H}_{\mathrm{BJ}}$ is, the larger reaction to $\dot{\boldsymbol{q}}_{\mathrm{B}}$ with respect to the same magnitude of $\dot{\boldsymbol{q}}_{\mathrm{J}}$ is gained. In this sense, $-\boldsymbol{H}_{\mathrm{BB}}^{-1}\boldsymbol{H}_{\mathrm{BJ}}$ represents the degree of mutual interference of $\dot{\boldsymbol{q}}_{\mathrm{B}}$ and $\dot{\boldsymbol{q}}_{\mathrm{J}}$ regarding the momenta.

On the other side, Equation (24) is also transformed as

$$\dot{\boldsymbol{q}}_{\mathrm{J}} = \boldsymbol{H}_{\mathrm{BJ}}^{\#}(\boldsymbol{h}_{\mathrm{B0}} - \boldsymbol{H}_{\mathrm{BB}}\dot{\boldsymbol{q}}_{\mathrm{B}}) + (\boldsymbol{1} - \boldsymbol{H}_{\mathrm{BJ}}^{\#}\boldsymbol{H}_{\mathrm{BJ}})\boldsymbol{\eta}, \tag{26}$$

where $\boldsymbol{A}^{\#}$ for an arbitrary matrix $\boldsymbol{A}$ means the Moore-Penrose's inverse matrix, and $\boldsymbol{\eta}$ is an arbitrary vector

of the corresponding size. $\mathbf{1} - \boldsymbol{H}_{\mathrm{BJ}}^{\#}\boldsymbol{H}_{\mathrm{BJ}}$ forms the kernel space of the map from $\dot{\boldsymbol{q}}_{\mathrm{J}}$ to $\dot{\boldsymbol{q}}_{\mathrm{B}}$, which is called *the reaction-null space*. This helps, for instance, to control the robot's hands without affecting the movement of the base link.

4. Dealing with contact mechanics

4.1. Contact wrench cone and contact wrench sum

Let us get back to the contact mechanics. Although Section 2.3 provided a mathematical formulation to deal with the structure-varying nature of the system due to the unilaterality and friction limit of contact forces, it is still difficult to synthesize the robot motion based on it. On the other hand, preferable locations and movements of the contact points are often designed in advance in the context of motion planning and control. If it is desired that the robot keeps the current contact points to be stationary, for example, the condition (15) is posed on all combinations of $\{(\dot{\boldsymbol{p}}_{Ck}, \boldsymbol{f}_{Ck})\}$ $(k = 1, \ldots, N_{\mathrm{C}})$. The set $\mathcal{F}_{\mathrm{C}}$ of possible net wrenches $\boldsymbol{\tau}_{\mathrm{C}}$ of the contact forces $\{\boldsymbol{f}_{Ck}\}$ that satisfy the condition is defined as

$$\mathcal{F}_{\mathrm{C}} = \left\{ \boldsymbol{\tau}_{\mathrm{C}} \middle| \boldsymbol{\tau}_{\mathrm{C}} = \begin{bmatrix} \boldsymbol{f}_{\mathrm{C}} \\ \boldsymbol{n}_{\mathrm{C}} \end{bmatrix} = \sum_{k=1}^{N_{\mathrm{C}}} \begin{bmatrix} \boldsymbol{f}_{Ck} \\ \boldsymbol{p}_{Ck} \times \boldsymbol{f}_{Ck} \end{bmatrix}, \right.$$
$$\left. \| \boldsymbol{f}_{Ck} - \left(\boldsymbol{v}_k^{\mathrm{T}} \boldsymbol{f}_{Ck} \right) \boldsymbol{v}_k \| \leq \mu_{Sk} \boldsymbol{v}_k^{\mathrm{T}} \boldsymbol{f}_{Ck} \right\}. \quad (27)$$

Hirukawa et al. [42] called the above $\boldsymbol{\tau}_{\mathrm{C}}$ and $\mathcal{F}_{\mathrm{C}}$ *the contact wrench sum* (CWS) and *the contact wrench cone* (CWC), respectively.

Suppose a certain set of $(\boldsymbol{q}, \dot{\boldsymbol{q}}, \ddot{\boldsymbol{q}}) = (\boldsymbol{q}^*, \dot{\boldsymbol{q}}^*, \ddot{\boldsymbol{q}}^*)$ that kinematically keeps all the contact points to be stationary is given through the inverse kinematics, and the upper limit of joint actuation torques is sufficiently large so that a constraint on $\boldsymbol{\tau}_{\mathrm{J}}$ can be omitted. A necessary condition for this motion to be dynamically consistent is that the equivalent inertial wrench $\boldsymbol{\tau}_{\mathrm{C}}^*$ to it is included in CWC. $\boldsymbol{\tau}_{\mathrm{C}}^*$ can be obtained from Equation (18) through the inverse dynamics. Hirukawa et al. [43] also proposed the following method to judge if a wrench is included in CWC. A set of an individual contact force $\boldsymbol{f}_{Ck}$ within the static friction limit forms an open cone, which is named *friction cone*, as depicted in Figure 2(a). An approximation of this by an open regular L-gonal pyramid, where L is a larger integer than 2, as Figure 2 (b) enables the following representation:

$$\boldsymbol{f}_{Ck} \in \left\{ \boldsymbol{f} \middle| \boldsymbol{f} = \sum_{l=1}^{L} \varepsilon_l (\boldsymbol{v}_k + \mu_{Sk} \boldsymbol{t}_{kl}), \forall \varepsilon_l \geq 0 \right\}, \quad (28)$$

where $\boldsymbol{t}_{kl}$ $(l = 1, \ldots, L)$ is a unit vector that points the lth vertex of a regular L-gon on an orthogonal plane to $\boldsymbol{v}_k$. This is named *span form* by Hirai [44]. A wrench $\boldsymbol{\tau}$ is included in CWC if and only if $\boldsymbol{\varepsilon}$ that satisfies the following conditions exists:

$$\boldsymbol{\tau} = \begin{bmatrix} \boldsymbol{L}_1 & \cdots & \boldsymbol{L}_{N_{\mathrm{C}}} \\ \boldsymbol{p}_{\mathrm{C}1} \times \boldsymbol{L}_1 & \cdots & \boldsymbol{p}_{\mathrm{C}N_{\mathrm{C}}} \times \boldsymbol{L}_{N_{\mathrm{C}}} \end{bmatrix} \boldsymbol{\varepsilon}, \quad \boldsymbol{\varepsilon} \geq \boldsymbol{0}, \quad (29)$$

where

$$\boldsymbol{L}_k \stackrel{\mathrm{def}}{=} \begin{bmatrix} \boldsymbol{l}_{k1} & \boldsymbol{l}_{k2} & \cdots & \boldsymbol{l}_{kL} \end{bmatrix} \quad (30)$$

$$\boldsymbol{l}_{kl} \stackrel{\mathrm{def}}{=} \boldsymbol{v}_k + \mu_{Sk} \boldsymbol{t}_{kl} \quad (31)$$

$$\boldsymbol{\varepsilon} \stackrel{\mathrm{def}}{=} \begin{bmatrix} \boldsymbol{\varepsilon}_1^{\mathrm{T}} & \cdots & \boldsymbol{\varepsilon}_{N_{\mathrm{C}}}^{\mathrm{T}} \end{bmatrix}^{\mathrm{T}} \quad (32)$$

$$\boldsymbol{\varepsilon}_k \stackrel{\mathrm{def}}{=} \begin{bmatrix} \varepsilon_{k1} & \cdots & \varepsilon_{kL} \end{bmatrix}^{\mathrm{T}}. \quad (33)$$

An existence of such $\boldsymbol{\varepsilon}$ can be checked by solving a linear programming to minimize $\sum_{k=1}^{N_{\mathrm{C}}} \sum_{l}^{L} \varepsilon_{kl}$ subject to Equation (29), for example.

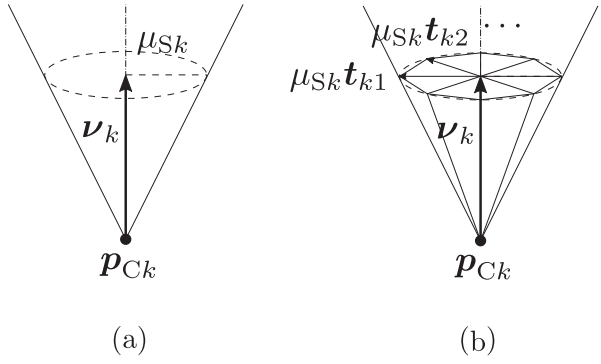

Figure 2. Friction cone and pyramidal approximation. (a) Friction cone and (b) pyramidal approximation of friction cone.

4.2. Zero-Moment point

The relationship between the contact force and motion is comprehensive in a particular case that all the contact points $\{\boldsymbol{p}_{Ck}\}$ $(k = 1, \ldots, N_{\mathrm{C}})$ are on an identical plane (the supporting plane) over which the static friction coefficient μ_{S} is uniform. The CWS $\boldsymbol{\tau}_{\mathrm{C}}$ in this case satisfies the following conditions:

$$\boldsymbol{v}^{\mathrm{T}} \boldsymbol{f}_{\mathrm{C}} \geq 0 \quad (34)$$

$$\| \boldsymbol{f}_{\mathrm{C}} - (\boldsymbol{v}^{\mathrm{T}} \boldsymbol{f}_{\mathrm{C}}) \boldsymbol{v} \| \leq \mu_{\mathrm{S}} \boldsymbol{v}^{\mathrm{T}} \boldsymbol{f}_{\mathrm{C}} \quad (35)$$

$$\boldsymbol{p}_{\mathrm{Z}} \in \mathcal{S} = \mathcal{CH}(\{\boldsymbol{p}_{Ck}\}) \quad (36)$$

$$\left| \boldsymbol{v}^{\mathrm{T}} (\boldsymbol{n}_{\mathrm{C}} - \boldsymbol{p}_{\mathrm{Z}} \times \boldsymbol{f}_{\mathrm{C}}) \right| \leq \mu_{\mathrm{S}} r_{\mathrm{C}} \boldsymbol{v}^{\mathrm{T}} \boldsymbol{f}_{\mathrm{C}}, \quad (37)$$

where $\boldsymbol{v}$ is the outward unit normal vector of the supporting plane, $\mathcal{CH}(\cdot)$ means the planar convex hull of

a specified set of points, r_C is a finite constant value depending on $\mathcal{S}$, and $\boldsymbol{p}_Z$ is the center of pressure (COP) defined as

$$\boldsymbol{p}_Z \stackrel{\text{def}}{=} \frac{\sum_{k=1}^{N_C}(\boldsymbol{v}^T\boldsymbol{f}_{Ck})\boldsymbol{p}_{Ck}}{\sum_{k=1}^{N_C}\boldsymbol{v}^T\boldsymbol{f}_{Ck}}. \tag{38}$$

Equation (34) means that the net normal force never attracts the robot to the supporting plane. This is derived by summing up the unilaterality conditions of the individual normal forces. When the equality holds, the robot floats in the air and free-falls. Equation (36) also comes from the unilaterality of the normal forces, and simply means that COP never goes out of the supporting region. Equations (35) and (37) come from the limitation of friction forces. If the total force applied to the robot exceeds the limitation, the robot slips.

$\mathcal{S}$ in Equation (36) is often called *the supporting region* or *the base of support*. The condition (36) equivalently represents the limitation of the reaction torque acting within the supporting region, which is directly related with tipping of the robot, and thus, is even more severe than the others. It is beneficial from several viewpoint that the condition can be geometrically interpreted based on a relationship between a point and a convex region. More importantly, the following identity holds:

$$\boldsymbol{p}_Z \equiv \frac{\boldsymbol{v}^T\boldsymbol{p}_O}{\boldsymbol{v}^T\boldsymbol{f}_C}\boldsymbol{f}_C + \frac{\boldsymbol{v}\times\boldsymbol{n}_C}{\boldsymbol{v}^T\boldsymbol{f}_C}, \tag{39}$$

where $\boldsymbol{p}_O$ is an arbitrary point on the supporting plane. The net contact force/torque is related with the centroidal momentum as Equations (18) and (19). The definition Equation (38) tells that COP is determined from distribution of the reaction forces resulted from motion. Equation (39) means that the same point can be related with the motion. Namely, COP $\boldsymbol{p}_Z^*$ corresponding to an intended motion $(\boldsymbol{q}^*, \dot{\boldsymbol{q}}^*, \ddot{\boldsymbol{q}}^*)$ can be predicted from the equivalent inertial wrench $\boldsymbol{\tau}_C^*$. This leads to an intuitive idea to plan or control motion such that $\boldsymbol{p}_Z^*$ is located within the planned transition of the supporting region in order to avoid tipping as Vukobratović and Juričić [45] pointed out.

It is confirmed that the tangential component of the torque about $\boldsymbol{p}_Z$ on the supporting plane (tipping torque) becomes zero, which made Vukobratović et al. [46] come up with *the Zero-moment point (ZMP)* as an alias of COP. Although it has been already acknowledged in the field, it is not an appropriate name in the authors' opinion because the normal component of the torque about the point is not necessarily zero. Caron et al. [47] more suitably renamed it for *the Zero-tilting Moment Point*, which is still abbreviated as ZMP.

Even in the cases where the contact points are ranged three dimensionally, the idea of ZMP is still available provided an appropriate projection of the actual contact points onto a virtual supporting plane. An arbitrary choice of this plane adds one more degree of freedom to ZMP on a spatial line that is parallel to $\boldsymbol{f}_C$ as meant by Equation (39). In other words, ZMP is actually not a point but a line, and accordingly, the condition Equation (36) should read

$$\{\boldsymbol{p}_Z\} \cap \mathcal{S} \neq \emptyset, \tag{40}$$

where $\mathcal{S}$ in this case is the convex hull of the projected contact points. Sugihara et al. [48] defined *the virtual horizontal plane* and presented a method to compute an approximate supporting region on it. Caron et al. [47] generalized the idea more to be applicable to motions with non-coplanar distributions of contact points.

It is stated in many publications that the robot is dynamically stable if ZMP is within the supporting region. The authors would like to present a notion that the above is totally wrong; it is not a condition about the stability but a natural constraint on the motion. Also, note that the stability is discussed based on the time evolution of the system, whereas ZMP is an instantaneous quantity.

5. COM-ZMP model

The reduced-order dynamics based on the centroidal dynamics and the aggregated contact mechanics by ZMP are reasonably associated with each other. Let us transform $\boldsymbol{n}_C$ in Equation (19) to the net contact torque about ZMP $\boldsymbol{n}_Z$ as

$$(\boldsymbol{p}_G - \boldsymbol{p}_Z)\times(\dot{\boldsymbol{h}}_L + m\boldsymbol{g}) = \boldsymbol{n}_Z - \dot{\boldsymbol{h}}_A. \tag{41}$$

The following equation is derived from the above Equation (41), two facts $\boldsymbol{v}\times\boldsymbol{n}_Z = \boldsymbol{0}$ and $\boldsymbol{h}_L = m\dot{\boldsymbol{p}}_G$, and an assumption $\boldsymbol{v}\times\dot{\boldsymbol{h}}_A \simeq \boldsymbol{0}$:

$$\ddot{\boldsymbol{p}}_G + \boldsymbol{g} = \zeta^2(\boldsymbol{p}_G - \boldsymbol{p}_Z), \tag{42}$$

where

$$\zeta^2 \stackrel{\text{def}}{=} \frac{\boldsymbol{v}^T(\ddot{\boldsymbol{p}}_G + \boldsymbol{g})}{\boldsymbol{v}^T(\boldsymbol{p}_G - \boldsymbol{p}_Z)}. \tag{43}$$

Equation (42) means that the acceleration of COM including that due to the gravity becomes parallel to a line that passes COM and ZMP. The definition of ζ Equation (43) is available if $\boldsymbol{v}^T(\boldsymbol{p}_G - \boldsymbol{p}_Z) > 0$, which holds in many situations. This is called *the COM-ZMP model*, which was derived by Mitobe et al. [49]. If the coordinate frame is defined such that z-axis is aligned with the direction of gravity, i.e. $\boldsymbol{g} = \begin{bmatrix}0 & 0 & g\end{bmatrix}^T$, where

$g = 9.8\text{m/s}^2$ is the acceleration due to the gravity, a componentwise representation of Equation (42) with $\boldsymbol{p}_\text{G} = \begin{bmatrix} x_\text{G} & y_\text{G} & z_\text{G} \end{bmatrix}^\text{T}$ and $\boldsymbol{p}_\text{Z} = \begin{bmatrix} x_\text{Z} & y_\text{Z} & z_\text{Z} \end{bmatrix}^\text{T}$ is obtained as

$$\ddot{x}_\text{G} = \zeta^2 (x_\text{G} - x_\text{Z}) \tag{44}$$

$$\ddot{y}_\text{G} = \zeta^2 (y_\text{G} - y_\text{Z}) \tag{45}$$

$$\ddot{z}_\text{G} + g \equiv \zeta^2 (z_\text{G} - z_\text{Z}). \tag{46}$$

Note that Equation (46) is an identity. $\boldsymbol{p}_\text{Z}$ employed in Equation (42) is different from ZMP if $\boldsymbol{v} \times \dot{\boldsymbol{h}}_\text{A} \neq \boldsymbol{0}$. Popovic et al. [50] distinguished this point from ZMP and named *the Centroidal Moment Pivot (CMP)*. The offset of ZMP from CMP produces the inertial torque about COM.

Figure 3 illustrates geometric relationships between COM, ZMP and CMP, which is naturally associated with an inverted pendulum. Actually, the resemblance of dynamics between a walking mechanism and an inverted pendulum was focused on by many researchers [32,51–60] since the early stage of the field of biped robots based on an intuition that a heavy upper body is carried by alternating light support legs with narrow footprints. In those studies, ZMP was supposed to be constraint at a point foot as a pivot, and a step meant discontinuous relocation of ZMP. Namely, the system only accepted intermittent manipulations of the input like a bang-bang control. The unforced system of Equation (42) that appears when supported by a single point foot has been deeply studied.

Let us conduct the mode analysis of the linearized system, i.e. with $\zeta \simeq \text{const}$. The state equation form of Equation (44) is

$$\frac{\text{d}}{\text{d}t} \begin{bmatrix} x_\text{G} \\ \dot{x}_\text{G} \end{bmatrix} = \begin{bmatrix} 0 & 1 \\ \zeta^2 & 0 \end{bmatrix} \begin{bmatrix} x_\text{G} \\ \dot{x}_\text{G} \end{bmatrix} + \begin{bmatrix} 0 \\ -\zeta^2 \end{bmatrix} x_\text{Z}, \tag{47}$$

which is diagonalized as

$$\frac{\text{d}}{\text{d}t} \begin{bmatrix} x_\text{D} \\ x_\text{C} \end{bmatrix} = \begin{bmatrix} \zeta & 0 \\ 0 & -\zeta \end{bmatrix} \begin{bmatrix} x_\text{D} \\ x_\text{C} \end{bmatrix} + \begin{bmatrix} -\zeta \\ \zeta \end{bmatrix} x_\text{Z}, \tag{48}$$

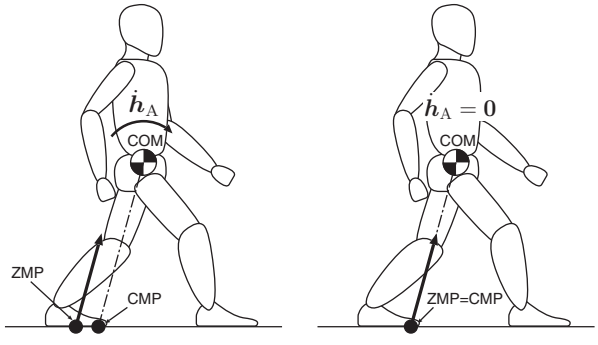

Figure 3. Geometric relationships of COM, ZMP and CMP.

where

$$\begin{aligned} x_\text{D} &\stackrel{\text{def}}{=} x_\text{G} + \dot{x}_\text{G}/\zeta \\ x_\text{C} &\stackrel{\text{def}}{=} x_\text{G} - \dot{x}_\text{G}/\zeta \end{aligned} \quad \Leftrightarrow \quad \begin{bmatrix} x_\text{G} \\ \dot{x}_\text{G} \end{bmatrix} = x_\text{D} \begin{bmatrix} 1 \\ \zeta \end{bmatrix} + x_\text{C} \begin{bmatrix} 1 \\ -\zeta \end{bmatrix}. \tag{49}$$

The above shows that the system has an unstable mode x_D and a stable mode x_C with respectively corresponding eigenvectors $\begin{bmatrix} 1 & \zeta \end{bmatrix}^\text{T}$ and $\begin{bmatrix} 1 & -\zeta \end{bmatrix}^\text{T}$. They were given another aliases *the convergent component of motion (CCM)* and *the divergent component of motion (DCM)*, respectively, by Takenaka et al. [61], and collectively referred as *Linear Inverted Pendulum Mode (LIPM)* by Kajita et al. [58]. Figure 4 shows the phase portrait of the system. Imanishi and Sugihara [62] found that the dimensionless system of the above was regarded as a scalar potential field, and named the function that defines the field *the LIPM potential*.

Kajita et al. [58] showed another aspect of the system. Equation (44) with the both sides multiplied by $\dot{x}_\text{G}$ and integrated over time turns to

$$\frac{1}{2}\dot{x}_\text{G}^2 - \frac{1}{2}\zeta^2 (x_\text{G} - x_\text{Z})^2 = E\text{: const.} \tag{50}$$

E is called *the orbital energy*. It led to a control strategy to engage the COM motion and foot-placements, namely, how to decide the timing to switch the pivot foot in order to continue walking with predetermined foot placements. Pratt et al. [63] dealt with the flip side of the problem in a particular case, namely, how to decide the foot placement x_CP in order to zero the orbital energy and stop walking. The answer is

$$x_\text{CP} \stackrel{\text{def}}{=} x_\text{G} + \dot{x}_\text{G}/\zeta, \tag{51}$$

which was named *the (Instantaneous) Capture Point*. It is in fact identical with *the Extrapolated COM (XCOM)*

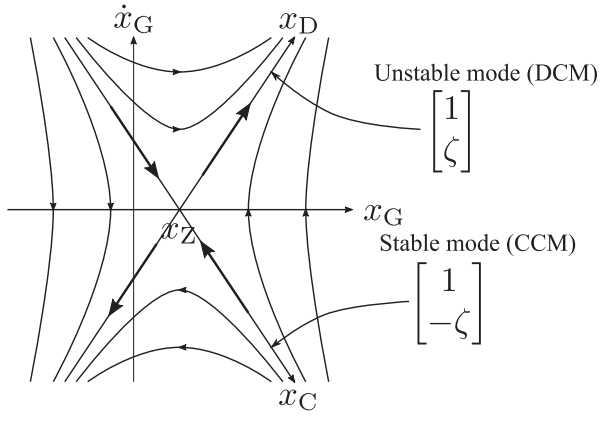

Figure 4. LIPM

proposed by Hof et al. [64]. The discussion has been deployed to the concept of *capturability* [65] for robots with non-zero-area soles and non-zero inertial torque about COM. Sugihara [66] studied how the stability of COM can be maximized with a feedback control, which covered the discussion about the Capture Point.

x_D defined by Equation (49) and x_{CP} by Equation (51) are apparently the same, and hence, some may think that DCM is identical with the Capture Point. However, it is actually a misunderstand. As depicted in Figure 5, the state $(x_G, \dot{x}_G)$ is projected to x_D- and x_C-axes, respectively. DCM and CCM are obtained by doubling those components, which is not relevant for the mode analysis since the modes are scale-invariant. On the other hand, the idea of the capture point is to shift the system such that x_C-axis passes the current state $(x_G, \dot{x}_G)$ by instantaneously relocating x_Z to x_{CP}. DCM vanishes as the result; in other words, the Capture Point captures DCM. In conclusion, DCM and the Capture Point are essentially different from each other, though they have the same mathematical form due to the symmetry of x_D- and x_C-axes with respect to x_G-axis.

Kajita et al. [58] also found that the system dynamics is strictly linearized if the movement of COM is artificially constrained on a spatial line. If the line passes a point above the pivot foot at a constant height h, Equation (44) turns to

$$\ddot{x}_G = \bar{\zeta}^2(x_G - x_Z), \tag{52}$$

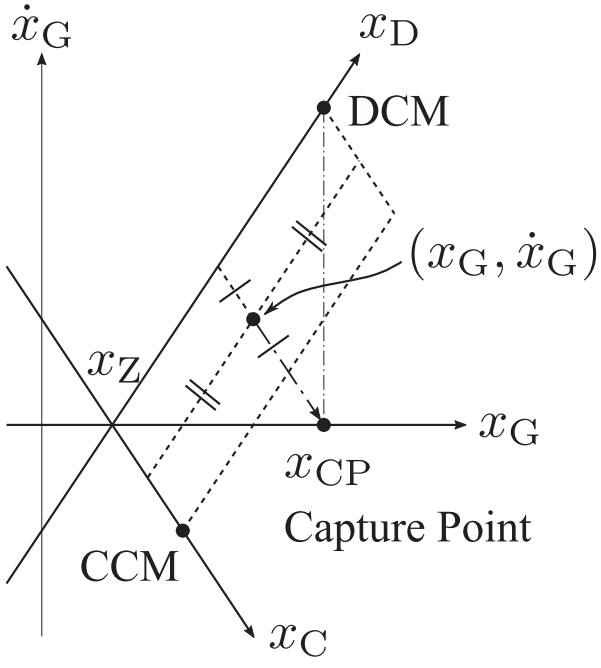

Figure 5. DCM and capture point.

where

$$\bar{\zeta} \stackrel{\text{def}}{=} \sqrt{\frac{g}{h}}: \text{const.} \tag{53}$$

Interestingly, the gradient of the line does not appear in the dynamics, meaning that the vertical position of COM can vary on the line while linearity of the system is preserved. The two-dimensional version was found by Sadao et al. [67,68], where the COM draws a hyperbolic curve on a spatial plane. A further study by Englsberger et al. [69] has revealed that it is a particular case of the system that the COM is constrained on a line, and it actually converges to the line. They also generalized the model to a three-dimensional version by replacing ZMP with another point with a vertical offset as

$$\ddot{\boldsymbol{p}}_G = \bar{\zeta}^2(\boldsymbol{p}_G - \boldsymbol{p}_R) \tag{54}$$

$$\boldsymbol{p}_R \stackrel{\text{def}}{=} \boldsymbol{p}_Z + \boldsymbol{g}/\bar{\zeta}^2. \tag{55}$$

$\boldsymbol{p}_R$ is called *the Virtual Repellent Point (VRP)*.

The point-foot model works for simplifying the control problem but reduces the potential mobility of robots. Raibert [56] proposed an idea of *virtual support point* in his theory for controlling legged machines in a unified way and made an interesting statement that it might enhance the mobility if the point would be variable with a non-zero-area supporting region. Currently, we can understand that the virtual support point is identical with ZMP and he seemed to predict the COM-ZMP model. Actually, the idea to manipulate ZMP has greatly helped many followers to devise motion planning and control schemes. Refer another survey paper [70]. It should be noticed, however, that the COM-ZMP model does not always represent the system dynamics appropriately. Some typical cases that the model does not fit are illustrated in Figure 6. If the contact points are distributed three-dimensionally, ZMP does not represent them in a comprehensive manner as Caron et al. [47] studied. If the robot is in the air, ZMP does not exist. If ZMP is close to

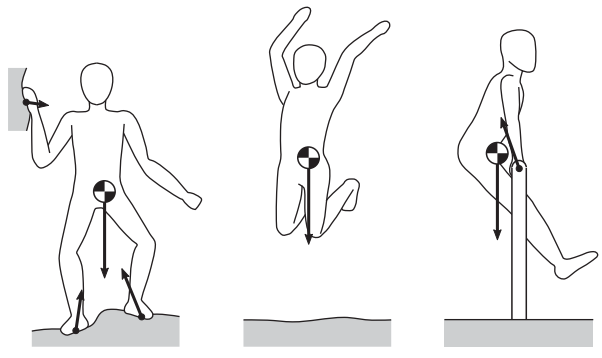

Figure 6. Cases that the COM-ZMP model does not fit.

COM, the inertial torque about COM is more dominant than that COM produces about ZMP.

6. Control frameworks to synthesize the whole-body motion

Fundamental mathematics to describe the dynamics of humanoid robots has been reviewed so far. This section gets one step further into a problem to synthesize the whole-body motion of the robot to the intended behavior based on the mathematics. The intention is represented by a set of requirements on the motion including a preferable time evolution of COM derived in the previous section and some other task-oriented partial movements of the body. A difficulty is that the number of requirements dynamically changes during motions due to the structure-varying nature. In addition, the requirements are not necessarily satisfiable mainly because of the limitation of contact forces. If there is no solution that satisfies all the requirements, they have to be compromised by a dynamically feasible motion with the priority of each requirement taken into account. A stack of the requirements in the order of priority from lowest to highest is called the Stack of Tasks (SoT)[94,95], and a computation of joint actuation torques from SoT is called the prioritized motion resolution. Though various control frameworks for this problem have been developed, in the authors' thought, they are classified into some groups.

Figure 7(a) shows the first group. The desired accelerations of COM $\ddot{\boldsymbol{p}}_{\mathrm{G}}^{*}$ and other body parts $\ddot{\boldsymbol{p}}_{\mathrm{E}}^{*}$ are determined from the motion references ${}^{\mathrm{d}}\boldsymbol{p}_{\mathrm{G}}$ and ${}^{\mathrm{d}}\boldsymbol{p}_{\mathrm{E}}$, respectively, supposing quadratically convergent time evolutions in many cases, and then, converted to dynamically feasible ones. The desired joint actuation torques $\boldsymbol{\tau}_{\mathrm{J}}^{*}$ and contact force $\boldsymbol{\tau}_{\mathrm{C}}^{*}$ are obtained during the process, whereas the latter is discarded. This is an enhancement of the operational space control [71] based on a natural idea to use the equation of motion. Yamane and Nakamura [6] named this concept *the dynamics filter* and proposed a method to utilize the null space in order to deal with the different priority. Sentis and Khatib [72] showed a more generalized form of computation using the null-space projectors. Nagasaka et al. [73] renamed this *the generalized inverse dynamics*, where they derived a sophisticated method to deal with the priority with slack variables. Further extensions have been made in order to solve multiple priorities in a hierarchical manner and increase the computational efficiency and robustness [74–77].

Figure 7(b) shows the second group, in which the desired contact force $\boldsymbol{\tau}_{\mathrm{C}}^{*}$ is determined first according to the style of force allocation [78], and then, converted to the desired joint actuation torques $\boldsymbol{\tau}_{\mathrm{J}}^{*}$ together with a virtual tracting force $\boldsymbol{\tau}_{\mathrm{E}}^{*}$ for contact-free body parts. This two-staged approach is based on the idea that the contact force works as an indirect input to the system, more specifically, to the centroidal momentum via Equation (18) as Fujimoto and Kawamura [79] pointed out. (a) and (b) are not clearly distinguished only from this viewpoint since some methods [74,76] in the group (a) also take this process internally. The essential difference between them is whether the conversion from the desired contact forces to the joint actuation torques is done based on the equation of motion, where the nonlinear effects are compensated, or on the virtual work principle as well as Pratt et al. [80], where the nonlinear effects are left. Hyon [81] presented the first implementation of this approach and explained that the passivity of the system is guaranteed with some assumptions. Ott et al. [82] proposed a more generalized method. Concerning with the mapping matrix for the force allocation, Hosokawa et al. [83] proposed the DCM generalized inverse, in which an effect for natural stabilization of the system is embedded, though it was used with the inverse dynamics framework (a) rather than (b).

While the ideas of (a) and (b) are convincing, they have a drawback that torque-controllable actuators are required in them, which are not easily available today. Figure 7(c) shows another approach where the desired time evolutions of COM $\boldsymbol{p}_{\mathrm{G}}^{*}$ with the limitation of contact forces taken into account is determined first based on the COM-ZMP model. It is resolved into the referential motion of joints $\boldsymbol{q}_{\mathrm{J}}^{*}$ together with the desired time evolutions of the other body parts $\boldsymbol{p}_{\mathrm{E}}^{*}$. The desired joint actuation torques $\boldsymbol{\tau}_{\mathrm{J}}^{*}$ are determined as to track it. If the desired motions of body parts are given in the dimension of velocity, it is an extension of the resolved motion rate control [84]. Or, if they are given as the referential positions and attitudes, it is done via the inverse kinematics. In whichever cases, the centroidal momentum matrices are exploited. Boulic et al. [36] called this class of motion resolution that figures in the mass distribution *the Inverse Kinetics*. Tamiya et al. [39,40] proposed a concept of *Auto-balancer*, which is similar to the dynamics filter but outputs the desired motions of joints. Sugihara et al. [37,48] proposed a more compact implementation based on the COM-ZMP model. Kajita et al. [35] proposed the resolved momentum control as an analogy of the resolved motion rate control. Kanoun et al. [85] proposed a method to deal with hierarchical multiple priorities. Efficient and robust solvers of the inverse kinematics have also been developed [86–88]. As described in the above, this approach has a longer history than (a) and (b) since it is applicable to robots with widely available low-backdrivable position-controlled actuators. Instead, a coupled effect of the movements of COM and extremities in contact with the environment has to be

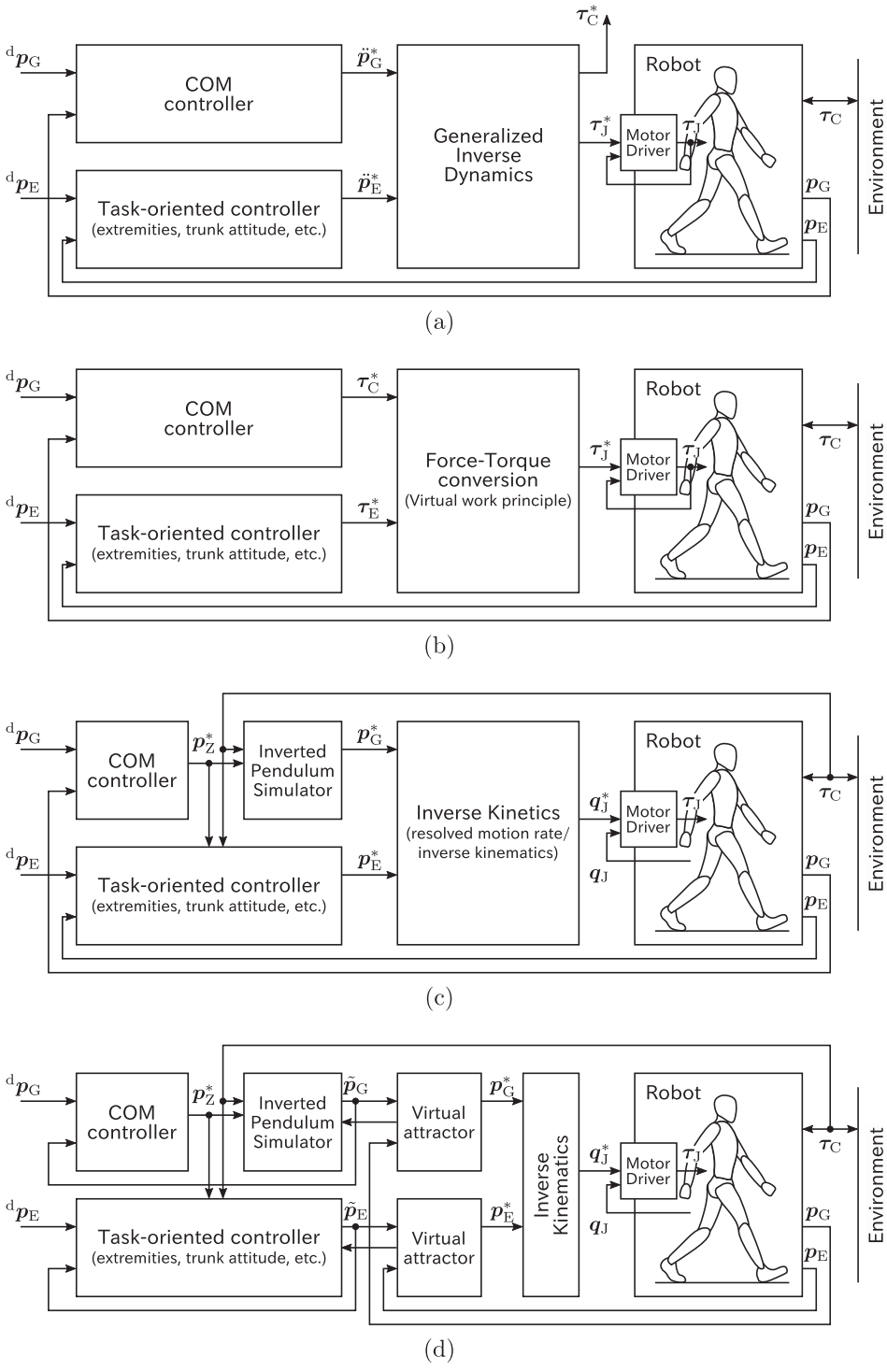

Figure 7. Different motion resolution control frameworks. (a) Generalized inverse dynamics. (b) Force-torque conversion (based on the virtual work principle). (c) Inverse kinetics and (d) Inverse kinematics with virtual attractor.

considered in this framework since the contact forces are gained via the latter, and the admittance control should be conducted on them, meaning that force sensors are required to be mounted on the extremities. Fujimoto and Kawamura [79] presented the first implementation conforming to this framework. Kajita et al. [89] proposed a method to decompose the tracking error of ZMP to the desired individual contact wrenches to be given to the admittance controller with a feedforward technique to compensate the delay of ZMP. Caron et al. [90] directly employed the net contact wrench that is equivalent with the desired centroidal dynamics including the desired

ZMP as the reference. Yamamoto [91] discussed this issue from another side by focusing on the motor controller. A preferable mechanical impedance of body parts in the task space that would be presented by the admittance controller can be equivalently converted to that in the joint space and implemented as a variable PD compensator for tracking $\boldsymbol{q}_{\mathrm{J}}^{*}$. This idea was named *Resolved Multiple-Viscoelasticity Control*.

A concern about solvability may arise in (c); note again that the desired motions of body parts are not necessarily achievable simultaneously. Although the prioritized motion resolution techniques [86,87] work for one-shot computations even in unsolvable cases, the supposed time evolution of the body parts might diverge due to the accumulation of error. Sato and Sugihara [92] discussed this point and proposed a framework to provide the system with more flexibility by introducing virtual attractors as shown in Figure 7(d). The referential motions of each body part are described as dynamical systems and connected with the actual body via the virtual attractor, which counteracts the referential motions and prevents growth of the gap between them.

The last part of this section is devoted to discuss an issue of how to set priorities. The requirements on the robot motion are classified as follows.

(A) Conserved linear/angular momentum
(B) Mechanical constraint (e.g. closed kinematic structure)
(C) Desired contact with the environment
(D) Desired (non-conserved) linear/angular momentum
(E) Desired motions of effectors in free-space

(A) is validated when the robot is in the air or supported only by a point or an edge. This is the strongest natural constraint since the robot behavior is ruled by this regardless of control. (B) is also a natural constraint but has a certain degree of tolerance due to backlashes or elastic deformations of body parts. Regarding (C), the contact points are not strictly constrained but might accept slight sliding on and detaching from the environment, though it is not desirable. (D) is an artificial constraint and is associated with the net force/torque that has to be consistent with the contact condition. It also has a tolerance depending on the supporting region. Allocation of contact points and manipulation of the net contact force are mutually dependent as seen in Section 4, and thus, their priorities are occasionally turned over. Nevertheless, they are less prioritized than (A) and (B). The remaining (E) is artificially given based on the task to be achieved and affects the performance of task executions. Though it is less prioritized than the physical security of the robot in many cases, there can be extreme situations where the robot has to accomplish tasks even by losing its balance, e.g. to catch a falling object by diving to it. Hence, the priority (E) compared to (C) and (D) depends on the context.

7. Conclusion

This paper reviewed how to describe kinematics and dynamics of a humanoid mechanism, how to represent contact mechanics, and how to synthesize the whole-body motion. Although the dynamics of humanoid robots is complex, many works have carefully built a mathematical foundation to discuss it.

The authors stated in the introduction that it is necessary to model the dynamics of humanoids in order to bring the human-like intelligence into engineering discussions. They believe that humans' intelligent behaviors are not so simple that they can be reproduced without any model. On the other hand, they are also aware that a controller that depends on a too much elaborated model rather reduces flexibility to disturbances of the robot, which is also another aspect of intelligence. While the efficacy of modeling the robot body as rigid kinematic chain has been acknowledged through countless studies, how to model the environment as a counterpart of the robot has not been thoroughly discussed, which might be a focus in future developments.

CWS and ZMP present convenient ways to check the consistency between a supposed contact condition and a supposed motion. They have been utilized in many sophisticated methods for motion planning, in which a preferable transition of the supporting points is given a priori. The transition of contact state, however, is the most dynamic aspect of the humanoid robots and is determined according to the time evolution of the system in the real world. It is also a concern that contact and non-contact are not clearly discriminated based on analog sensory information. A real-time controller that directly handles the transition of contact state is always demanded. Some stochastic techniques [93] to deal with the contact might help it.

It is still controversial which is advantageous to do the motion resolution based on the inverse dynamics or the inverse kinematics. The authors predict that it will take more time to conclude this. A key is the availability of torque-controlled actuators.

Highly advanced computers have encouraged computationally expensive optimizations to be embedded in a real-time control loop as a common technique. The authors personally worry that it has rather discouraged researchers to pay attention to the dynamics of humanoid

robots. They would like to note that it is always important to figure out the essence of system dynamics in order to understand humans' motion skill and implement it on robots.

Disclosure statement

No potential conflict of interest was reported by the authors.

Notes on contributors

Tomomichi Sugihara is a researcher of Preferred Networks, Inc. He received his Ph.D. from the University of Tokyo in 2004. He was an academic research assistant from April 2004 to February 2005 in the University of Tokyo, and became a research associate. He had worked at Kyushu University as a guest associate professor from 2007 to 2010, and at Osaka University as an associate professor from 2010 to 2019. His research interests include kinematics and dynamics computation, motion planning, control, hardware design, and software development of anthropomorphic robots. He also studies human motor control based on robotics technologies. He is a member of IEEE.

Mitsuharu Morisawa is a researcher of the Intelligent Systems Research Institute, AIST from 2004. He received his Ph.D. from Keio University, Japan, in 2004. He was a visiting researcher at the LAAS-CNRS, France from 2009 to 2010, and an invited researcher at INRIA Rhone-Alpes, France in 2011. Since 2020, he is a deputy director of the Cooperative Research Laboratory at the CNRS-AIST JRL (Joint Robotics Laboratory), UMI3218/IRL. His research interests include the whole body and multi-contact locomotion and its stabilization control of humanoid robots. He is a member of IEEE.

Funding

This work was supported by Ministry of Education, Culture, Sports, Science and Technology [Grant-in-Aid for Scientific Research (B), #18H0331].

References

[1] Sugihara T. Dynamics of humanoid robots. J Robot Soc Jpn. 2018;36(2):95–102.
[2] Vukobratović M, Stepanenko J. Mathematical models of general anthropomorphic systems. Math Biosci. 1973;17(3–4):191–242.
[3] Vafa Z, Dubowsky S. On the dynamics of manipulators in space using the virtual manipulator approach. Proceedings of the 1987 IEEE International Conference on Robotics and Automation. 1987. p. 579–585.
[4] Umetani Y, Yoshida K. Resolved motion rate control of space manipulators with generalized jacobian matrix. IEEE Trans Robot Automat. 1989;5(3):303–314.
[5] Fujimoto Y, Kawamura A. Three dimensional digital simulation and autonomous walking control for eight-axis biped robot: Proceedings of the 1995 IEEE International Conference on Robotics and Automation. 1995. p. 2877–2884.
[6] Nakamura Y, Yamane K. Dynamics computation of structure-Varying kinematic chains and its application to human figures. IEEE Trans Robot Automat. 2000;16(2):124–134.
[7] Yoshida K, Nenchev DN, Uchiyama M. Moving base robotics and reaction management control. Proceedings of the Seventh International Symposium of Robotics Research. 1995. p. 100–109.
[8] Walker MW, Orin DE. Efficient dynamic computer simulation of robotic mechanisms. Trans ASME J Dyn Syst Measure Control. 1982;104:205–211.
[9] Whitney DE. The mathematics of coordinated control of prosthetic arms and manipulators. Trans ASME J Dyn Syst Measure Control. 1972;G-94(4):303–309.
[10] Orin DE, Schrader WW. Efficient computation of the jacobian for robot manipulators. Int J Robot Res. 1984;3(4):66–75.
[11] Hertz H. Über die Berührung fester elastischer Körper und über die Harte. Gesammelte Werke J. A. Barth Leipzig. 1895;1:174–196.
[12] Hunt KH, Crossley FRE. Coefficient of restitution interpreted as damping in Vibroimpact. Trans ASME J Appl Mech. 1975;42(2):440–445.
[13] Dahl PR. A solid friction model. Aerospace Corporation, 1968. (Technical Report: TOR-0158(3107-18)-1.
[14] Canudas deWit C, Olsson H, Aström KJ, et al. A new model for control of systems with friction. IEEE Trans Automat Control. 1995;40(3):419–425.
[15] Wakisaka N, Sugihara T. Loosely-constrained volumetric contact force computation for rigid body simulation. Proceedings of the 2017 IEEE/RSJ International Conference on Intelligent Robots and Systems. 2017. p. 6428–6433.
[16] Moreau JJ, Panagiotopoulos PD. Nonsmooth mechanics and applications. Springer-Verlag; 1988. (CISM Courses and Lectures; 302).
[17] Moreau JJ. Quadratic programming in mechanics: dyna mics of one sided constraints. SIAM J Control. 1966;4(1):153–158.
[18] Lötstedt P. Numerical simulation of time-Dependent contact and friction problems in rigid body mechanics. SIAM J Sci Stat Comput. 1984;5(2):370–393.
[19] Moore M, Wilhelms J. Collision detection and response for computer animation. Comput Graphics. 1988;22(4):289–298.
[20] Baraff D. Analytical methods for dynamic simulation of non-penetrating rigid bodies. Comput Graphics. 1989;23(3):223–232.
[21] Anitescu M, Potra FA. Formulating dynamic multi-rigid-body contact problems with friction as solvable linear complementarity problems. Report on Computational Mathematics No. 93. The University of Iowa. 1996.
[22] Stewart DE, Trinkle JC. An implicit time-stepping scheme for rigid body dynamics with inelastic collisions and coulomb friction. Int J Numer Methods Eng. 1996;39:2673–2691.
[23] Fujimoto Y, Kawamura A. Simulation of an autonomous biped walking robot including environmental force interaction. IEEE Robot Automat Mag. 1998;5(2):33–41.
[24] Kokkevis E. Practical physics for articulated characters. Proceedings of Game Developers Conference. 2004.
[25] Lacoursière C. Regularized; stabilized; variational methods for multibodies. Proceedings of the 48th Scandinavian Conference on Simulation and Modeling. 2007. p. 40–48.

[26] Aubin J-P, Cellina A. Differential inclusions, set-valued maps and viability theory. Vol. 264 of Grundlehren der mathematischen wissenschaften, Springer-Verlag Berlin Heidelberg; 1984.
[27] Stewart DE. Existence of solutions to rigid body dynamics and the Painlevé paradoxes. Comptes Rendus de l'Académie des Sciences – Series I – Mathematics. 1997;325(6):689–693.
[28] Génot F, Brogliato B. New results on Painlevé paradoxes. Euro J Mech A/Solids,. 1999;18(4):653–677.
[29] Sugihara T, Nakamura Y. Balanced micro/macro contact model for forward dynamics of rigid multibody. Proceedings of the 2006 IEEE International Conference on Robotics and Automation. 2006. p. 1880–1885.
[30] Todorov E. A convex, smooth and invertible contact model for trajectory optimization. Proceedings of the 2011 IEEE International Conference on Robotics and Automation. 2011. p. 1071–1076.
[31] Wakisaka N, Sugihara T. Fast and reasonable contact force computation in forward dynamics based on momentum-level penetration compensation. Proceedings of the 2014 IEEE/RSJ International Conference on Intelligent Robots and Systems, 2014. p. 2434–2439.
[32] Miyazaki F, Arimoto S. A control theoretic study on dynamical biped locomotion. Trans ASME J Dyn Syst Measure Control. 1980;102:233–239.
[33] Furusho J, Masubuchi M. Control of a dynamical biped locomotion system for steady walking. Trans ASME J Dyn Syst Measure Control. 1986;108:111–118.
[34] Orin DE, Goswami A, Lee S -H. Centroidal dynamics of a humanoid robot. Auton Robots. 2013;35:161–176.
[35] Kajita S, Kanehiro F, Kaneko K, et al. Resolved momentum control: humanoid motion planning based on the linear and angular momentum. Proceedings of the 2003 IEEE/RSJ International Conference on Intelligent Robots and Systems. 2003. p. 1644–1650.
[36] Boulic R, Mas R, Thalmann D. A robust approach for the center of mass position control with inverse kinetics. J Comput Graphics. 1996;20(5):693–701.
[37] Sugihara T. Mobility enhancement control of humanoid robot based on reaction force manipulation via whole body motion [Ph.D dissertation]. The University of Tokyo, 2004.
[38] Morita Y, Ohnishi K. Attitude control of hopping robot using angular momentum. Proceedings of the 2003 IEEE International Conference on Industrial Technology. 2003. p. 173–178.
[39] Tamiya Y, Inaba M, Inoue H. Realtime balance compensation for dynamic motion of full-Body humanoid standing on one leg (in Japanese). J Robot Soc Jpn. 1999;17(2):268–274.
[40] Kagami S, Kanehiro F, Tamiya Y. AutoBalancer: an online dynamic balance compensation scheme for humanoid robots. In: Donald BR, Lynch KM. and Rus D. editors, Algorithmic and computational robotics: new directions: the Fourth Workshop on the Algorithmic Foundations of Robotics. A. K. Peters/CRC Press; 2001. p. 329–339.
[41] Yoshida K, Nenchev DN. A general formulation of underactuated manipulator systems. Proceedings of the Eighth International Symposium of Robotics Research. 1997. p. 33–44.
[42] Hirukawa H, Hattori S, Kajita S, et al. A pattern generator of humanoid robots walking on a rough terrain. Proceedings of the 2007 IEEE International Conference on Robotics and Automation. 2007. p. 2181–2187.
[43] Hirukawa H, Hattori SHarada, Kaneko K, et al. A universal stability criterion of the foot contact of legged robots – adios ZMP. Proceedings of the 2006 IEEE International Conference on Robotics and Automation. 2006. p. 1976–1938.
[44] Hirai S. Analysis and planning of manipulation using the theory of polyhedral convex cones [Ph.D. dissertation]. Kyoto University; 1991.
[45] Vukobratović M, Juričić D. Contribution to the synthesis of biped gait. IEEE Trans Biomed Eng. 1969;BME-16(1):1–6.
[46] Vukobratović M, Stepanenko J. On the stability of anthropomorphic systems. Math Biosci. 1972;15(1):1–37.
[47] Caron S, Pham Q, Nakamura Y. ZMP support areas for multicontact mobility under frictional constraints. IEEE Trans Robot. 2017;33(1):67–80.
[48] Sugihara T, Nakamura Y, Inoue H. Realtime humanoid motion generation through ZMP manipulation based on inverted pendulum control. Proceedings of the 2002 IEEE International Conference on Robotics and Automation. 2002. p. 1404–1409.
[49] Mitobe K, Capi G, Nasu Y. Control of walking robots based on manipulation of the zero moment point. Robotica. 2000;18(6):651–657.
[50] Popovic M, Goswami A, Herr HM. Ground reference points in legged locomotion: definitions, biological trajectories and control implications. Inter J Robot Res. 2005;24(12):1013–1032.
[51] Witt DC. A feasibility study on automatically-controlled powered lower-limb prostheses. Technical report of the University of Oxford; 1970.
[52] Vukobratović M, Frank AA, Juričić D. On the stability of biped locomotion. IEEE Trans Biomed Engin. 1970;BME-17(1):25–36.
[53] Chow CK, Jacobson DH. Further studies of human locomotion: postural stability and control. Math Biosci. 1972;15(1):93–108.
[54] Yamashita T, Yamada M, Inotani H. A fundamental study of walking (in Japanese). Biomechanics. 1972;1:226–234.
[55] Gubina F, Hemami H, McGhee RB. On the dynamic stability of biped locomotion. IEEE Trans Biomed Engin. 1974;BME-21(2):102–108.
[56] Raibert MH. Legged robots that balance. Cambridge: MIT Press; 1986.
[57] Kitamura S, Kurematsu Y, Nakai Y. Application of the neural network for the trajectory planning of a biped locomotive robot. Neural Netw. 1988;1(1):344.
[58] Kajita S, Yamaura T, Kobayashi A. Dynamic walking control of a biped robot along a potential energy conserving orbit. IEEE Trans Robot Automat. 1992;8(4):431–438.
[59] Minakata H, Hori Y. Realtime speed-changeable biped walking by controlling the parameter of virtual inverted pendulum. Proceedings of the 20th Annual Conference of IEEE Industrial Electronics. 1994.
[60] Miyakoshi S, Cheng G. Examining human walking characteristics with a telescopic compass-like biped walker model. Proceedings of the 2004 IEEE International

Conference on System, Man and Cybernetics. 2004. p. 1538–1543.
[61] Takenaka T, Matsumoto T, Yoshiike T. Real time motion generation and control for biped robot – 1st report: walking gait pattern generation –. Proceedings of the 2009 IEEE/RSJ International Conference on Intelligent Robots and Systems. 2009. p. 1084–1091.
[62] Imanishi K, Sugihara T. Autonomous biped stepping control based on the LIPM potential. Proceedings of the 2018 IEEE-RAS International Conference on Humanoid Robots. 2018. p. 593–598.
[63] Pratt J, Carff J, Drakunov S, et al. Capture point: a step toward humanoid push recovery. Proceeding of the 2006 IEEE-RAS International Conference on Humanoid Robots. 2006. p. 200–207.
[64] Hof AL, Gazendam MGJ, Sinke WE. The condition for dynamic stability. J Biomech. 2005;38:1–8.
[65] Koolen T, de Boer T, Rebula J, et al. Capturability-based analysis and control of legged locomotion, part 1: theory and application to three simple gait models. Inter J Robot Res. 2012;31(9):1094–1113.
[66] Sugihara T. Standing stabilizability and stepping maneuver in planar bipedalism based on the best COM-ZMP regulator. Proceedings of the 2009 IEEE International Conference on Robotics and Automation. 2009. p. 1966–1971.
[67] Sadao K, Hara T, Yokokawa R. Dynamic control of biped locomotion robot for disturbance on lateral plane (in Japanese). Proceedings of the 72nd JSME Kansai Annual Meeting. 1997. p. 10.37–10.38.
[68] Kajita S, Matsumoto O, Saigo M. Real-time 3D walking pattern generation for a biped robot with telescopic legs. Proceeding of the IEEE International Conference on Robotics and Automation. 2001. p. 2299–2036.
[69] Englsberger J, Ott C, Albu-Schïffer A. Three-Dimensional bipedal walking control based on divergent component of motion. IEEE Trans Robot. 2015;31(2):355–368.
[70] Yamamoto K, Kamioka T, Sugihara T. Survey on model-based control for humanoid balancing, walking, hopping and running. Advanced Robotics (under review).
[71] Khatib O. A unified approach for motion and force control of robot manipulators: the operational space formulation. Inter J Robot Automat. 1987;RA-3(1):43–53.
[72] Sentis L, Khatib O. Control of free-floating humanoid robots through task prioritization. Proceedings of the 2005 IEEE International Conference on Robotics and Automation. 2005. p. 1730–1735.
[73] Nagasaka K, Kawanami Y, Shimizu S, et al. Whole-body cooperative force control for a two-armed and two-wheeled mobile robot using generalized inverse dynamics and idealized joint units. Proceedings of the 2010 IEEE International Conference on Robotics and Automation. 2010. p. 3377–3383.
[74] Righetti L, Buchli J, Mistry M, et al. Optimal distribution of contact forces with inverse dynamics control. Inter J Robot Res. 2013;32(3):280–298.
[75] Wensing PM, Orin DE. Generation of dynamic humanoid behaviors through task-space control with conic optimization. Proceedings of the 2013 IEEE International Conference on Robotics and Automation. 2013. p. 3103–3109.
[76] Herzog A, Righetti L, Grimminger F, et al. Balancing experiments on a torque-controlled humanoid with hierarchical inverse dynamics. Proceedings of the 2014 IEEE/RSJ International Conference on Intelligent Robots and Systems. 2014. p. 981–988.
[77] Del Prete A, Nori A, Metta G, et al. Prioritized motion-force control of constrained fully-actuated robots: "Task space inverse dynamics". Robot Auton Syst. 2015;63:150–157.
[78] Sreenivasan S, Waldron K, Mukherjee S. Globally optimal force allocation in active mechanisms with four frictional contacts. J Mech Design. 1996;118(3):353–359.
[79] Fujimoto Y, Obata S, Kawamura A. Robust biped walking with active interaction control between foot and ground. Proceedings of the 1998 IEEE International Conference on Robotics and Automation. 1998. p. 2030–2035.
[80] Pratt J, Dilworth P, Pratt G. Virtual model control of a bipedal walking robot. Proceedings of the 1997 IEEE International Conference on Robotics and Automation. 1997. p. 193–198.
[81] Hyon S-H. Compliant terrain adaptation for biped humanoids without measuring ground surface and contact forces. IEEE Trans Robot. 2009;25(1):171–178.
[82] Ott C, Roa MA, Hirzinger G. Posture and balance control for biped robots based on contact force optimization. Proceedings of the 2011 IEEE-RAS International Conference on Humanoid Robots. 2011. p. 206–233.
[83] Hosokawa M, Nenchev DN, Hamano T. The DCM generalized inverse: efficient bodywrench distribution in multi-contact balance control. Adv Robot. 2018;32(14):778–792.
[84] Whitney DE. Resolved motion rate control of manipula tors and human prostheses. IEEE Trans Man-Machine Syst. 1969;10(2):47–53.
[85] Kanoun O, Lamiraux F, Wieber P-B, et al. Prioritizing linear equality and inequality systems: application to local motion planning for redundant robots. in Proceedings of the 2009 IEEE International Conference on Robotics and Automation. 2009. p. 2939–2944.
[86] Sugihara T. Solvability-unconcerned inverse kinematics by the levenberg-Marquardt method. IEEE Trans Robot. 2011;27(5):984–991.
[87] Sugihara T. Robust solution of prioritized inverse kinematics based on hestenes-powell multiplier method. Proceedings of the 2014 IEEE/RSJ International Conference on Intelligent Robots and Systems. 2014. p. 510–515.
[88] Escande A, Mansard N, Wieber P-B. Hierarchical quadra tic programming: fast online humanoid-robot motion generation. Int J Robot Res. 2014;33(7):1006–1028.
[89] Kajita S, Morisawa M, Miura K, et al. Biped walking stabilization based on linear inverted pendulum tracking. Proceedings of the 2010 IEEE/RSJ International Conference on Intelligent Robots and Systems. 2010. p. 4489–4496.
[90] Caron S, Kheddar A, Tempier O. Stair climbing stabilization of the HRP-4 humanoid robot using whole-body admittance control. Proceedings of the 2019 IEEE International Conference on Robotics and Automation. 2019. p. 277–283.
[91] Yamamoto K. Resolved multiple-Viscoelasticity control for a humanoid. IEEE Robotics and Automation Lett. 2017;3(1):44–51.

[92] Sato RK, Sugihara T. Walking control for feasibility at limit of kinematics based on virtual leader-follower. Proceedings of the 2017 IEEE-RAS International Conference on Humanoid Robots. 2017. p. 718–723.
[93] Rotella N, Schaal S, Righetti L. Unsupervised contact learning for humanoid estimation and control. arXiv: 1709.07472. 2017.
[94] Yamane K, Nakamura Y. Dynamics filter – concept and implementation of on-line motion generator for human figures. Proceedings of the 2000 IEEE International Conference on Robotics and Automation. 2000. p. 688–695.
[95] Mansard N, Stasse O, Evrard P, et al. A versatile Generalized Inverted Kinematics implementation for collaborative working humanoid robots: The Stack Of Tasks); IEEE International Conference on Advanced Robotics; 2009.